Glucagon-Like Peptide 1 Receptor Agonist Stimulation Inhibits Laser-Induced Choroidal Neovascularization by Suppressing Intraocular Inflammation

Akira Machida,[1] Keiji Suzuki,[2] Takafumi Nakayama,[2] Sugao Miyagi,[1] Yuki Maekawa,[1,3] Ryuya Murakami,[1] Masafumi Uematsu,[1] Takashi Kitaoka,[1,4] and Akio Oishi[1]

[1]Department of Ophthalmology and Visual Sciences, Graduate School of Biomedical Sciences, Nagasaki University, Nagasaki, Nagasaki Prefecture, Japan
[2]Department of Radiation Medical Sciences, Atomic Bomb Disease Institute, Nagasaki University, Nagasaki, Nagasaki Prefecture, Japan
[3]Department of Ophthalmology, National Hospital Organization Nagasaki Medical Center, Nagasaki, Nagasaki Prefecture, Japan
[4]Department of Ophthalmology, Syunkai-kai Inoue Hospital Eye Center, Nagasaki, Nagasaki Prefecture, Japan

Correspondence: Akira Machida, Department of Ophthalmology and Visual Sciences, Nagasaki University, Sakamoto 1-7-1, Nagasaki, Nagasaki Prefecture 852-8102, Japan; a-machida@nagasaki-u.ac.jp.

Received: November 22, 2024
Accepted: April 16, 2025
Published: May 7, 2025

Citation: Machida A, Suzuki K, Nakayama T, et al. Glucagon-like peptide 1 receptor agonist stimulation inhibits laser-induced choroidal neovascularization by suppressing intraocular inflammation. *Invest Ophthalmol Vis Sci.* 2025;66(5):15. https://doi.org/10.1167/iovs.66.5.15

Purpose. The glucagon-like peptide-1 receptor (GLP-1R), a diabetes therapy target, is expressed in multiple organs and is associated with neuroprotective, anti-inflammatory, and antitumor effects, particularly in cardiac and cerebral tissues. Although GLP-1's role in diabetic and ischemic retinopathies is well-studied, its influence on choroidal neovascularization (CNV) in exudative age-related macular degeneration (AMD) remains unclear. This study explored the effects of GLP-1 on CNV using a laser-induced mouse model.

Methods. The anti-angiogenic effects of GLP-1 were tested using ex vivo sprouting assays in 3-week-old C57BL/6J mice. In 6-week-old mice, GLP-1R localization in laser-induced CNV lesions was analyzed via immunohistochemistry. Liraglutide, a GLP-1R agonist, was administered subcutaneously for 7 days or by single intravitreal injection post-laser. Eyeballs collected on days 1 to 7 post-laser were analyzed using RT-qPCR for GLP-1R expression and inflammatory cytokines.

Results. GLP-1R-positive cells were detected in CNV lesions and were expressed in Iba-1-positive activated microglia or macrophages. They also expressed in abnormal retinal pigment epithelial cells and surrounding normal endothelial cells. NOD-like receptor protein 3 (NLRP3) inflammasome signaling was observed near CNV. Liraglutide inhibited angiogenesis in ex vivo assays and significantly reduced CNV formation with both subcutaneous and intravitreal administration. Additionally, Liraglutide inhibited expression of NLRP3, IL-1β, IL-6, and TNF expression compared with healthy controls. Intravitreal GLP-1R antagonist reduced subcutaneous effects.

Conclusions. Liraglutide suppresses CNV formation, likely via NLRP3 inflammasome inhibition. Intraocular GLP-1R appears to mediate anti-CNV effects, supporting GLP-1R agonists as potential adjunctive therapy for exudative AMD and warranting further investigation into its safety and clinical feasibility.

Keywords: age-related macular degeneration (AMD), choroidal neovascularization (CNV), glucagon-like peptide-1 receptor (GLP-1R) agonists, glucagon-like peptide-1 receptor (GLP-1R) expression, laser-induced mice model, intravitreal injection, nucleotide oligomerization domain-like receptor protein 3 (NLRP3), reverse transcription polymerase chain reaction (RT-PCR), sprouting assay, subcutaneous injection

Age-related macular degeneration (AMD) is a leading cause of visual impairment in developed countries.[1–3] The atrophic form is characterized by gradual macular atrophy, with anti-complement therapies recently developed to decelerate its progression. In the exudative form, overexpression of vascular endothelial growth factor-A (VEGF-A) promotes neovascularization and vascular permeability, leading to recurrent exudates, hemorrhage, and damage to photoreceptor cells, resulting in vision loss. Intravitreal anti-VEGF injections, including ranibizumab, aflibercept, brolucizumab, and faricimab, significantly improve visual outcomes[4–8]; however, they carry risks such as endophthalmitis and retinal detachment[9,10] and require frequent treatments, creating financial and logistical burdens.[11] Therefore, alternative therapies are needed.

Glucagon-like peptide-1 (GLP-1), an incretin hormone, was first identified in monkfish islets in 1981.[12] It enhances glucose-dependent insulin secretion, lowering

blood glucose in humans and animal models.[13,14] GLP-1 receptor (GLP-1R) agonists and dipeptidyl peptidase-4 (DPP-4) inhibitors are central in diabetes treatment.[15,16] GLP-1R is expressed beyond the pancreas, including in the brain, heart, and kidneys.[17] Whereas GLP-1 has a short half-life[18] due to DPP-4 degradation, long-acting GLP-1R agonists extends systemic activation, offering benefits like reduced cardiovascular risk and neuroprotection.[19–21]

GLP-1R is also expressed in the eyes,[22,23] particularly in ganglion cells and nerve fiber layers.[24] In vitro studies confirm its presence in retinal pigment epithelial (RPE)[25] cells and retinal endothelial cells.[26] Animal studies have shown GLP-1's benefits in diabetic retinopathy,[27–33] oxygen-induced retinopathy,[34] and ischemia-reperfusion injury.[35,36] Its anti-inflammatory[37–39] effects involve suppression of the NOD-like receptor protein 3 (NLRP3) inflammasome.[40,41] which is implicated in choroidal neovascularization (CNV) models, where inhibition reduces CNV size.[42–44]

We hypothesized that GLP-1R agonist administration mitigates CNV in AMD by suppressing inflammation. Given their well-established safety profile, flexible administration routes, and broad metabolic benefits, GLP-1-based therapies hold promise for non-diabetic applications.[21] If validated for preventing AMD onset and progression, these therapies could ease the treatment burden on patients. This study explored GLP-1's therapeutic potential in AMD by assessing GLP-1R expression and inflammatory markers in a laser-induced CNV mouse model.

Methods

Animals

Three- and 6-week-old C57BL/6J mice (Japan SLC, Inc., Shizuoka, Japan) were used in accordance with the Association for Research in Vision and Ophthalmology and Nagasaki University's Animal Experimentation Guidelines. Ethical approval was obtained from the Institutional Review Board at Nagasaki University Graduate School of Medicine. Mice were housed under a 12-hour light/12-hour dark cycle throughout the study.

Sprouting Assay

The sprouting assay, an ex vivo model of angiogenesis in AMD research,[45,46] was conducted using RPE/choroid/sclera tissue from 3-week-old mice. Tissue sections (1 mm × 1 mm) were cultured in 24-well plates embedded in 30 µL of Growth Factor Reduced Matrigel (BD Biosciences, Franklin Lakes, NJ, USA). The medium (Complete Medium Kit with Serum and Cultureboost-R, KAC CO., Ltd., Kyoto, Japan) was supplemented with 100 to 1000 nmol/L human GLP-1R agonist (Liraglutide, Victoza, Novo Nordisk A/S, Bagsværd, Denmark) or 100 ng/mL Recombinant Mouse VEGFR1/Flt-1 Fc Chimera Protein, CF (FUJIFILM Wako Pure Chemical Corporation, Osaka, Japan), as previously described.[47,48] The medium was changed every 2 days. Furthermore, clodronate-encapsulated liposomes SMALL (Funakoshi Co., Ltd., Tokyo, Japan) were added to the culture medium at a concentration of 100 µg/mL for the first 2 days of culture to promote macrophage depletion.[49,50] On day 6, images were acquired using the BIOREVO BZ-9000 microscope (Keyence Corporation, Osaka, Japan), and sprouting areas were quantified with ImageJ (version 2.14.0/1.54f).[51] Detached tissues within Matrigel were excluded from the analysis.

Induction of CNV

Laser-induced CNV, a model replicating the inflammatory pathogenesis of neovascular (exudative) AMD[52,53] was induced in 6-week-old mice. Anesthesia was administered intraperitoneally with 80 mg/kg ketamine HCl and 10 mg/kg xylazine. Pupils were dilated using 5% phenylephrine hydrochloride/0.8% tropicamide (SandolP, ROHTO NITTEN Co., Ltd., Nagoya, Japan), and Slip glasses were applied for stabilization. Laser photocoagulation was performed at 2 to 3 disk diameters from the optic disk using a slit-lamp system (MC-300, Nidek Corporation, Gamagori, Japan; wavelength = 647 nm; power = 150 mW; duration = 50 ms; and spot size = 70 µm).

For CNV measurements, 4 laser spots were used; 10 spots were used for expression analyses. Cavitation bubbles, marking Bruch's membrane disruption, served as endpoints. Laser spots were excluded based using established protocols[54]: (1) immediate bleeding > 2 × optic nerve diameter, (2) fusion with other lesions, (3) scars >5 × average size, or (4) bleeding scars or connections at the endpoint. Eyes exhibiting vitreous hemorrhage were excluded to limit the impact of intraocular inflammation.

Treatments

Liraglutide was administered via subcutaneous injection (SCI) or intravitreal (IV) injection. In the SCI group, mice received daily saline or Liraglutide (250, 500, or 1000 µg/kg) injections on the dorsal skin immediately after laser photocoagulation. In the IV injection group, mice received either phosphate-buffered saline (PBS) or Liraglutide (0.1–6.0 µg/eye/µL) into the vitreous humor immediately post-laser. The 0.1-µg dose, a 60-fold dilution of the product, was determined based on prior GLP-1R agonist studies[27,28] in rats. Single IV injection administration was performed using an Ito Special Compatible Needle, 33 Gauge, 15 mm, Type A (GL Sciences, Tokyo, Japan).

To assess ocular GLP-1R involvement, exendin 9-39 amide (Abcam plc, Cambridge, UK)[55] was injected intravitreally at a dose of 2 µg/eye/µL or 1 µL of PBS immediately after laser treatment. VEGFR1/Flt-1 Fc chimera protein, a positive anti-angiogenic control, was administered intravitreally at a dose of 10 ng/eye/µL. All IV injections were performed once with the mice under anesthesia immediately post-laser.

Immunohistochemistry

Mice were euthanized 7 days after laser treatment. Eyes were flat-mounted, sectioned on ice, and fixed in 10% formalin. Paraffin-embedded sections were cut to 3-µm thickness and stained for microscopic observation. Fluorescence observation materials are provided in Supplementary Table S1.

Antigen retrieval was performed by incubating slides in a 95°C water bath for 40 minutes in Tris-EDTA buffer (pH 9.0; Nichirei Bioscience, Tokyo, Japan). After PBS washes, the samples were incubated at 20°C to 25°C for 2 hours with the primary antibody and 1 hour with the secondary antibody, both diluted in TBS-DT (20 mM Tris-HCl, 137 mM NaCl, and pH 7.6, containing 50 mg/mL skim milk and 0.1% Tween-20). Slides were mounted with PBS containing 10% glycerol and 1 µg/mL diamidino-2-phenylindole. Fluorescent images were captured using a DM-6000B microscope and a DFC-350 FX digital camera (Leica, Wetzlar, Germany).

Choroidal Neovascularization Analyses

To measure the CNV area, the eyes were collected on day 7 post-laser and fixed in 4% paraformaldehyde in PBS for 30 minutes at 4°C. The cornea, iris, and lens were removed by sectioning at the corneal limbus on ice, and the vitreous and retina were extracted to create flat-mount specimens. After fixation at 20°C to 25°C for 60 minutes with Blocking One (Nacalai Tesque, Inc., Kyoto, Japan), then they were incubated overnight at 4°C with Anti-Mouse CD102. After three 10-minute washes, Alexa Fluor 488 was applied at 20°C to 25°C for 60 minutes. The antibody buffer contained 5% Blocking One and 0.05% Tween 20 in PBS. Samples were washed three more times and mounted on slides. CNV images were captured using a BIOREVO BZ-9000 fluorescence microscope (Keyence Corporation), and areas were measured using ImageJ software.

Reverse Transcription and Real-Time PCR

In the ex vivo sprouting assay, the RPE/choroid/sclera complex embedded in Matrigel was cultured for 6 days, then enzymatically dissociated using dispase at 37°C for 2 hours. Tissues and sprouts were separated via pipetting and homogenization to isolate target cells. In laser CNV models, total mRNA was extracted from RPE/choroid/sclera with retina at baseline (day 0) and days 1, 3, and 7 post-laser using the NucleoSpin RNA XS kit (Takara Bio Inc., Shiga, Japan) per the manufacturer's protocol. RNA concentration and purity were evaluated with a NanoDrop spectrophotometer (ThermoFisher Scientific, Waltham, MA, USA). Single-stranded cDNA was synthesized from DNaseI-treated RNA using the PrimeScript RT reagent Kit (Takara Bio Inc.). The RT-qPCR was performed using a LightCycler 480 System II (F. Hoffmann-La Roche Ltd., Switzerland) for 40 cycles, with 2 µL cDNA in a 20 µL reaction volume using TB Green Premix DimerEraser (Takara Bio Inc.) and gene-specific primers (details in Supplementary Table S2). The PCR protocol included 50°C for 2 minutes, 95°C for 30 seconds, and then followed by 40 cycles of 95°C for 5 seconds, 55°C for 30 seconds, and 72°C for 30 seconds. Melt curve analysis was performed by heating samples to 95°C at 0.11°C per second after incubation at 95°C for 5 seconds and 60°C for 1 minute. Non-single-peak Tm values were excluded. Reactions were performed in duplicate, and experiments were repeated at least twice. Cycle threshold (Ct) values were analyzed using the $\Delta\Delta$Ct method[56] and normalized to β-actin.

Body Weight and Blood Glucose Levels

In 6-week-old C57BL/6J mice treated with Liraglutide, the body weight and blood glucose levels were monitored. Liraglutide was administered subcutaneously at 1000 µg/kg daily at 11:00 AM. Blood glucose was measured at 0, 6, 12, 24, 36, and 48 hours post-treatment, and then every 24 hours until day 7. Body weights were recorded daily at 24-hour intervals. Blood glucose was measured using LAB Gluco (Funakoshi Co., Ltd.), calibrated specifically for mice.

Statistics

Data are presented as mean ± standard deviation. For CNV PCR, body weight, and glucose comparisons between treatment and control groups, the Mann–Whitney U test was used. Multiple-group comparisons were evaluated using the Kruskal–Wallis test, followed by Bonferroni-corrected Mann–Whitney U tests. Analyses were conducted using Easy R, a biostatistics-specific R (version 4.2.0) commander.[57] Significance was set at $P < 0.05$. All experimental procedures—including culture, laser treatment, specimen preparation, imaging, and PCR—were conducted by author Akira Machida. Data analysis was performed in a blinded manner by authors Sugao Miyagi and Ryuya Murakami.

Results

Ex Vivo Anti-Angiogenic Analysis by Sprouting Assay

The anti-angiogenic effect of Liraglutide was evaluated using an ex vivo sprouting assay on the mouse RPE/choroid/sclera complex ($n = 25$). Representative images from the control and treatment groups are shown in Figures 1A and 1B. In the negative control, the mean sprouting area was 2.47 ± 0.33 mm^2, serving as the baseline (Fig. 1C). Low-dose Liraglutide (100 nmol/L) reduced the area to 2.23 ± 0.46 mm^2, but the change was not significant ($P = 0.270$). In contrast, high-dose Liraglutide (1000 nmol/L) significantly reduced the area to 1.92 ± 0.44 mm^2 ($P < 0.001$), demonstrating a strong anti-angiogenic effect. FLT-1 Fc (100 ng/mL), the positive control, reduced the area to 1.69 ± 0.45 mm^2. As shown in Figure 1D, adding clodronate-encapsulated liposomes for 2 days significantly decreased the sprouting vessel area ($P = 0.035$), and Liraglutide's effect was no longer evident ($n = 10$). RT-qPCR revealed reduced Il-1β, TNFα, and NLRP3 expression after clodronate-liposome treatment, with no significant changes observed with Liraglutide (Fig. 1E).

Expression Analysis of GLP-1R in Paraffin Sections

To validate antibody specificity, staining images of untreated mouse pancreatic islets are shown in Supplementary Figure S1. Consecutive sections stained under identical conditions as the isotype control confirmed specific labeling of pancreatic β-cells.

GLP-1R and NLRP3 expression was examined in paraffin-embedded retinal sections from the mice on day 7 post-laser. Isotype controls are shown in Figures 2A to 2D. These sections revealed RPE rupture, labeled with cytokeratin 8/18 (CK8/18), confirming CNV induction. GLP-1R was broadly expressed (Figs. 2E–H), with strongest fluorescence in photoreceptor outer segments—regions affected by autofluorescence. GLP-1R was also detected in nerve fibers near the ganglion cell layer (GCL), outer plexiform layer (OPL), parts of the RPE, and choroidal vascular endothelium. Specific expression was identified in spindle-shaped Iba-1-positive cells within the CNV, suggesting activated microglia or macrophages (Figs. 2I–L).

NLRP3 was observed throughout the retina, with strong localization in the GCL, inner nuclear layer (INL), RPE, and CNV-associated spindle-shaped cells. Several NLRP3-positive cells co-expressed Iba-1 (Figs. 2M–P), supporting their identity as immune cells.

Expression Analysis of GLP-1R and NLRP3 in Flatmount

Paraffin-embedded flatmount sections with CNV lesions are shown in Figure 3. GLP-1R-positive cells (see Figs. 3A, 3B)

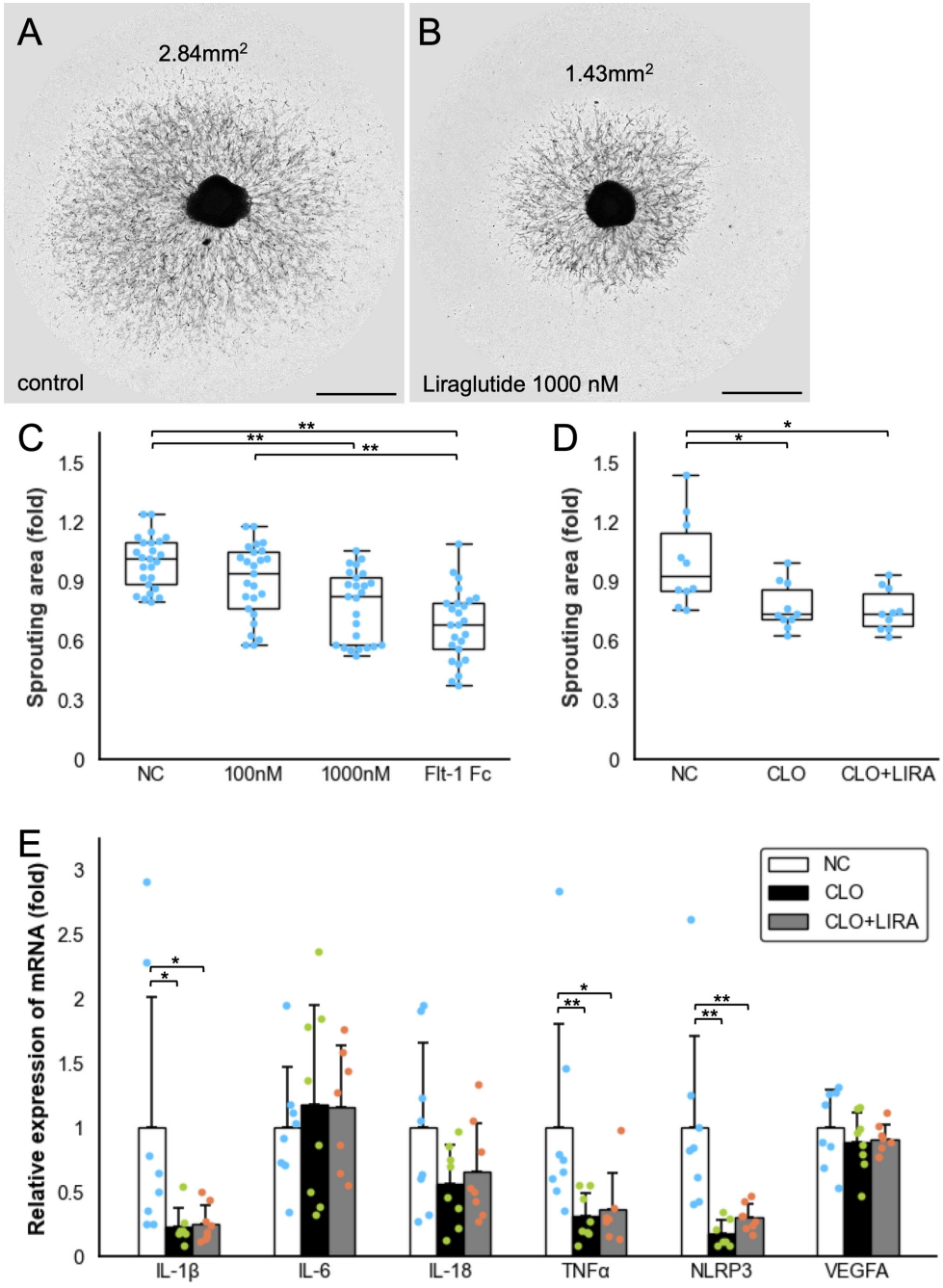

Figure 1. Representative images of RPE/choroid/sclera tissues and sprouting vessels on day 6 of culture. (**A**) Control group cultured in medium alone; sprouting area measured at 2.84 mm^2 using ImageJ software. (**B**) Group treated with 1000 nM Liraglutide; sprouting area measured at 1.43 mm^2. Scale bar = 1 mm. (**C**) Box-and-whisker plot comparing sprouting areas in the negative control (NC), Liraglutide (100 nM, and 1000 nM), and VEGFR1/Flt-1 Fc (100 µg/mL) groups ($n = 25$). Sprouting areas expressed as fold change versus control. Boxes show interquartile range (IQR); lines indicate median; whiskers extend to values within 1.5 × IQR. (**D**) Box-and-whisker plot comparing NC, clodronate liposomes (CLO, 100 µL/mL), and CLO + Liraglutide (1000 nM) groups ($n = 10$). (**E**) Bar chart of relative mRNA expression in sprouting tissues (RT-PCR) from the same groups as in **D** ($n = 8$). Data shown as mean ± SD. The P values were calculated using the Mann–Whitney U test with Bonferroni correction. *$P < 0.05$; **$P < 0.01$. IL, interleukin; NLRP3, NOD-like receptor protein 3; TNF, tumor necrosis factor; VEGFA, vascular endothelial growth factor A.

were observed in laser-induced abnormal RPE regions, strongly stained with CK8/18 (see Figs. 3C, 3D). Among CD31-positive endothelial cells, newly formed endothelial cells within the lesion lacked GLP-1R, whereas surrounding physiological choroidal endothelial cells expressed it (see Figs. 3E, 3F). GLP-1R-positive cells in the lesion were predominantly Vim-positive, indicating mesenchymal origin (see Figs. 3G, 3H).

NLRP3 staining showed strong nuclear signals within and around the lesion (see Figs. 3A, 3B). A cluster of intensely positive cells in the lower right was suspected to be lymphatic cells near the Harderian gland.

Investigative Ophthalmology & Visual Science

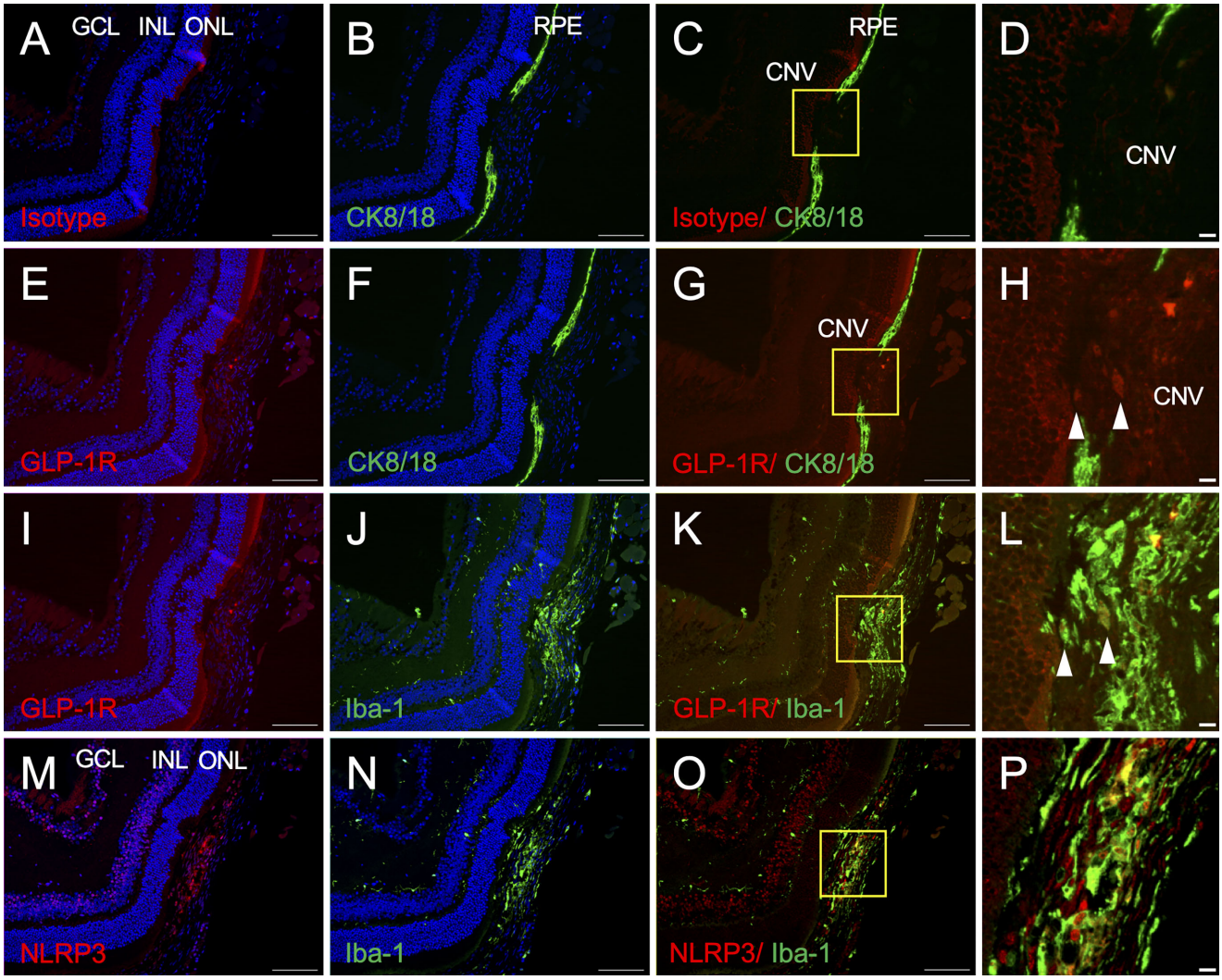

Figure 2. Fluorescent staining of paraffin-embedded mouse retina sections post-laser treatment shows isotype control images in panels (**A** to **D**), GLP-1R expression (*red*) in (**E to L**), and NLRP3 expression in (**M–P**); CK8/18 highlights RPE structure and rupture zones, with *green*, indicating CK8/18 or Iba-1 as labeled; magnified views in **D**, **H**, **L**, and **P** correspond to *yellow-boxed* regions in **C**, **G**, **K**, and **O**, respectively, and *arrows* in **H** and **L** mark representative spindle-shaped GLP-1R-positive cells in the CNV area; scale bars are 10 µm for **D**, **H**, **L**, and **P**, and 100 µm for the other panels. CK8/18, cytokeratin 8/18; CNV, choroidal neovascularization; GCL, ganglion cell layer; GLP-1R, glucagon-like peptide-1 receptor; Iba-1, ionized calcium-binding adapter molecule 1; INL, inner nuclear layer; NLRP3, NOD-like receptor protein 3; ONL, outer nuclear layer; RPE, retinal pigment epithelium.

Figures 3K and 3L show NLRP3-positive round cells in the RPE co-expressing Iba-1, suggesting undifferentiated or migrating monocytes. Within the lesion, NLRP3/Iba-1 co-positive cells surrounded by vimentin likely represent spindle-shaped microglia (see Figs. 3M–P). Granular NLRP3 near the laser scar likely indicates laser-induced inflammation.

Inhibition of CNV Formation by GLP-1R Agonist

In the CNV model, the target was set to exceed 50 effective scars; in all groups (Fig. 4), the mean was 19.3 ± 3.8 eyes and 54.6 ± 4.5 scars. Liraglutide significantly suppressed CNV formation in laser-induced mice (see Fig. 4A). Daily SCI of Liraglutide reduced CNV area from 20,080 ± 9259 µm^2 (control) to 15,340 ± 7584 µm^2 at 250 µg/kg (P = 0.048). Higher doses showed greater suppression: 13,232 ± 6635 µm^2 at 500 µg/kg and 11,491 ± 5729 µm^2 at 1000 µg/kg (both $P < 0.001$). This effect was inhibited by IV of Exendin9-39 amide, a GLP-1R antagonist (18,906 ± 8816 vs. 13,128 ± 8660 µm^2, $P < 0.001$; see Fig. 4B).

IV injections of Liraglutide also reduced the CNV area in a dose-dependent manner (see Fig. 4C). PBS-treated eyes had a mean CNV area of 21,145 ± 8558 µm^2, which decreased to 16,895 ± 6072 µm^2 for 0.1 µg ($P = 0.056$), 15,789 ± 6519 µm^2 for 0.6 µg ($P = 0.018$), and 13,433 ± 6366 µm^2 for 6.0 µg ($P < 0.001$). The VEGFR1/Flt-1 Fc group had a CNV area of 11,937 ± 4914 µm^2, comparable to 6.0 µg Liraglutide. Figures 4D to 4J present CD102-stained flat mounts showing optic nerves and CNV lesions with magnified lesion views.

Reduction of MRNA Expressions After GLP-1R Agonist Treatment

RT-qPCR of the RPE/choroid/sclera complex from day 0 to 7 post-laser showed that SCI of Liraglutide significantly

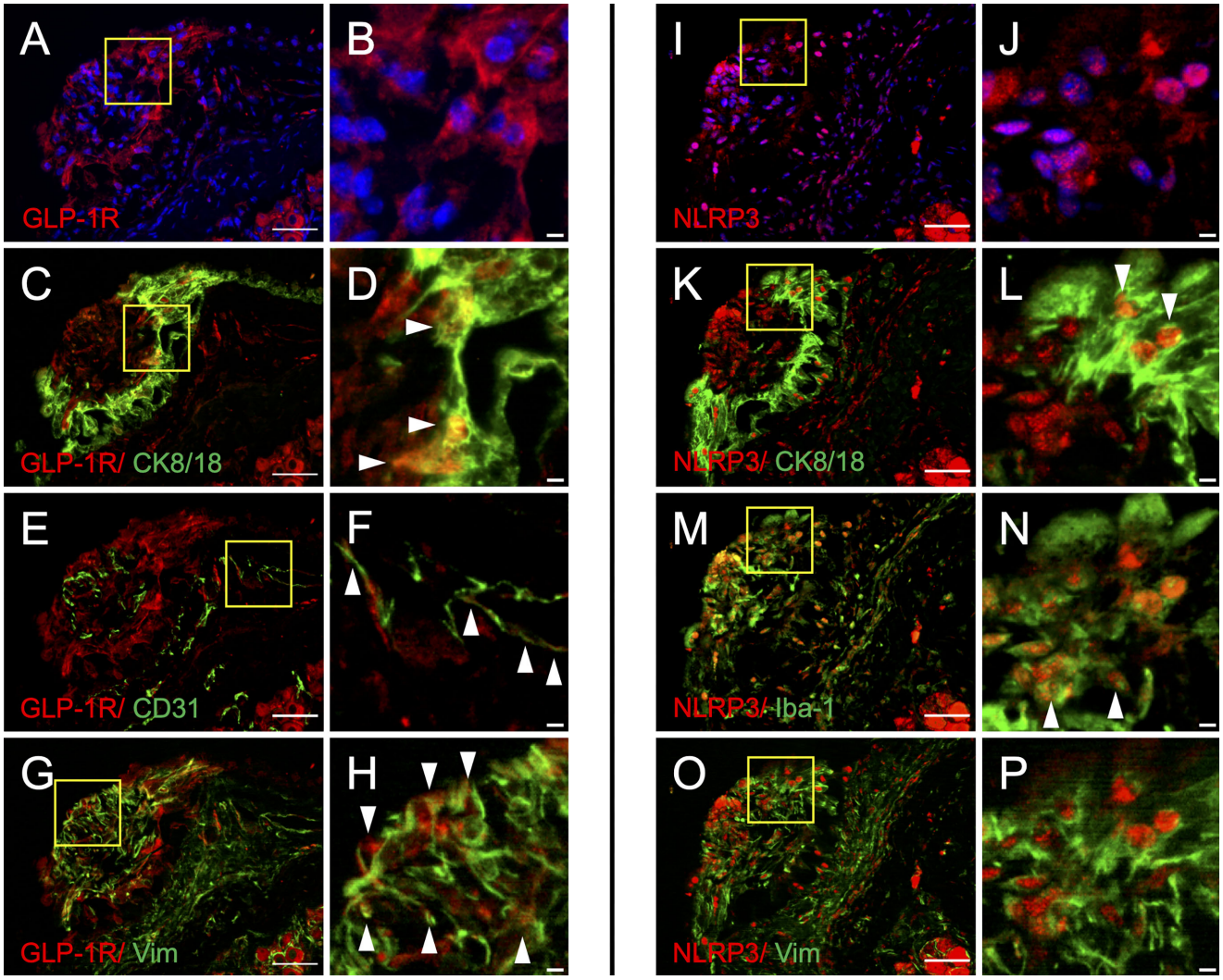

Figure 3. Fluorescent images of paraffin-embedded flat-mounted mouse eye sections on day 7 post-laser show red staining for GLP-1R in (**A–H**) and for NLRP3 in (**I–P**); in **C**, CK8/18 highlights the RPE, and **D** provides a magnified view near the laser scar with arrowhead indicating GLP-1R-positive abnormal RPE; in **E**, endothelial cells are stained with CD31, and **F** shows a magnified view of GLP-1R-positive vascular endothelial cells; **G** shows Vim staining, and **H** highlights GLP-1R-positive cells within CNV (*arrowheads*); **L**, **N**, and **P** are magnified views illustrating NLRP3-positive cells at the laser scar with CK8/18, Iba-1, and Vim staining, respectively; *arrowheads* in **L** and **N** mark nuclei of abnormal RPE and NLRP3/Iba-1 co-expressing cells within the CNV; scale bars = 10 µm (magnified images), 100 µm (others). CD31, cluster of differentiation 31; CK8/18, cytokeratin 8/18; CNV, choroidal neovascularization; GLP-1R, glucagon-like peptide-1 receptor; Iba-1, ionized calcium-binding adapter molecule 1; NLRP3, NOD-like receptor protein 3; RPE, retinal pigment epithelium; Vim, vimentin.

reduced IL-1β, IL-6, and TNF on day 1 ($P = 0.005$, $P = 0.038$, and $P = 0.020$, respectively), except for IL-18 (Figs. 5A–D). Although NLRP3 expression remained unchanged on day 1, it was significantly suppressed on day 3 ($P = 0.021$; Fig. 5E). Liraglutide had no notable effects on VEGFA or PLGF, but migration-associated factors, such as CXCL12 and AIF2, tended to increase without reaching statistical significance (Figs. 5F–I). GLP-1R expression levels remained unaffected (see Fig. 5H).

Changes in Body Weight and Blood Glucose Levels With GLP-1R Agonist Administration

High-dose Liraglutide (1000 µg/kg) led to rapid body weight loss from day 1 to day 3, followed by partial recovery (Fig. 6A). On day 7, the body weight remained significantly lower than the controls ($P < 0.001$). Blood glucose decreased at 6 hours post-treatment and persisted until 12 hours, rising by 24 hours before decreasing again with re-administration (Fig. 6B). Glucose levels remained above 70 mg/dL throughout the study, and no severe hypoglycemic symptoms were observed.

Discussion

Expression of GLP-1R in Mice

This study is the first to report GLP-1R-positive cells within laser-induced CNV scars in a mouse model. GLP-1R has been associated with inflammation-related immune cells in various organs.[58] We hypothesize that the GLP-1R-positive cells in CNV scars are microglia or macrophages activated by abnormal proliferation and inflammation,

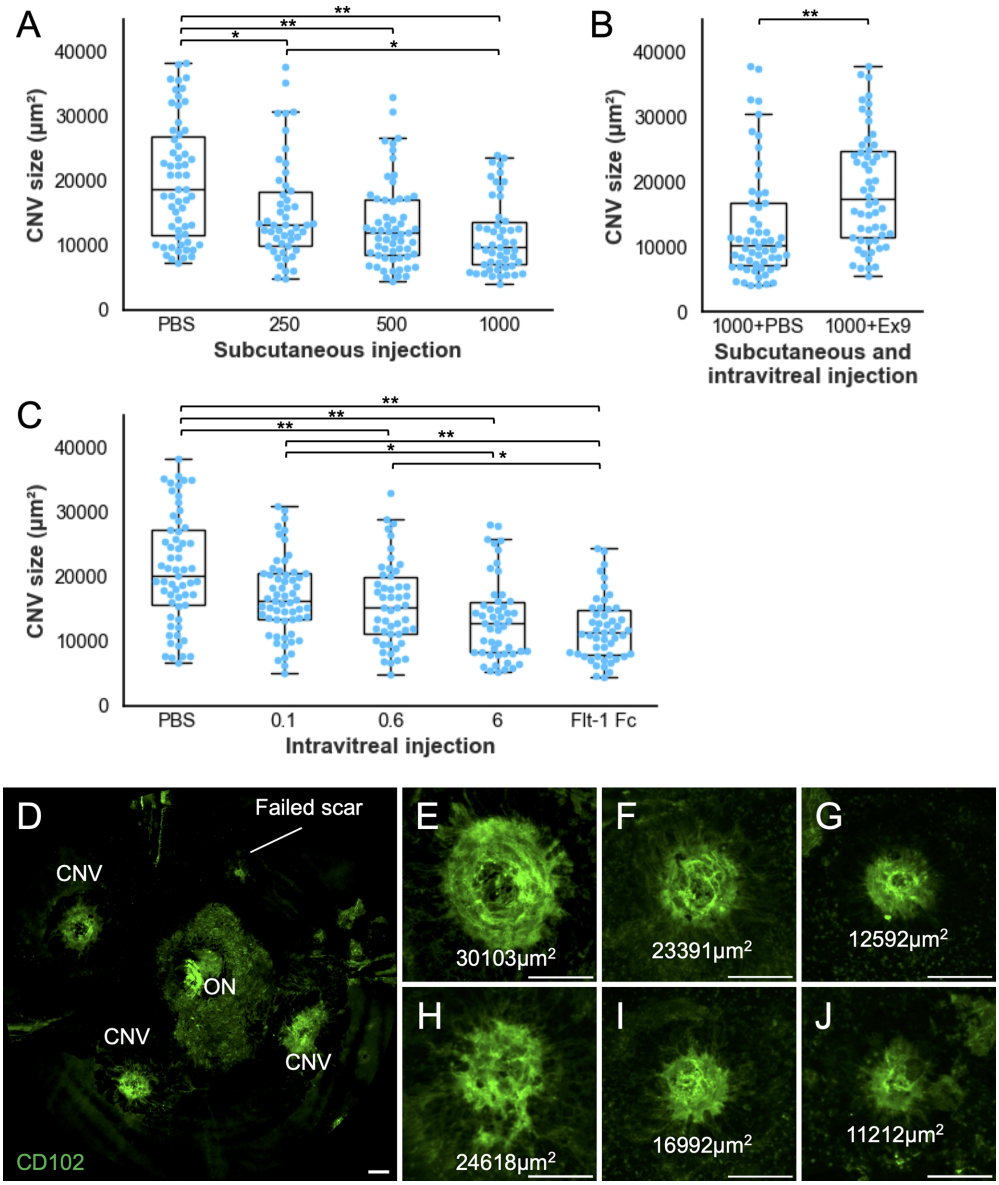

Figure 4. Box-and-whisker plots showing CNV area changes 7 days after laser photocoagulation in the CNV mouse model (n = 19.3 ± 3.8 eyes, and 54.6 ± 4.5 scars per group). (**A**) Shows CNV area after daily subcutaneous injections (SCIs) of PBS or Liraglutide at 250, 500, and 1000 μg/kg, (**B**) shows CNV area after SCI of Liraglutide at 1000 μg/kg combined with a single intravitreal (IV) injection of PBS or GLP-1R antagonist Ex9 (Exendin 9-39 amide, 2 μg/eye), and (**C**) shows CNV area following single IV injections of PBS, Liraglutide (0.1, 0.6, or 6 μg), or Flt-1 Fc (VEGFR1/Flt-1 Fc chimera protein, 10 ng). Boxes represent the interquartile range (IQR); *horizontal lines* indicate the median; whiskers extend to values within 1.5 × IQR. Data are presented as means ± SD, with P values from Mann–Whitney U test and Bonferroni correction, and statistical significance indicated by $^*P < 0.05$ and $^{**}P < 0.01$; (**D**) presents representative flat-mounts stained with CD102 showing the optic nerve and CNV lesions, including three successful CNV formations and one failed scar due to incomplete Bruch's membrane disruption; (**E–J**) show magnified CNV lesions with areas of 30,103 μm² (**E**, control), 23,301 μm² (**F**, SCI 250 μg/kg), 12,592 μm² (**G**, SCI 1000 μg/kg), 24,618 μm² (**H**, SCI 1000 μg/kg and IV Ex9), 16,992 μm² (**I**, IV 6 μg), and 11,212 μm² (**J**, IV Flt-1 Fc); scale bar = 100 μm. CD102, cluster of differentiation 102; CNV, choroidal neovascularization; GLP-1R, glucagon-like peptide-1 receptor; ON, optic nerve; PBS, phosphate-buffered saline; VEGFR1, vascular endothelial growth factor receptor 1.

based on immunohistochemistry findings. GLP-1R was also observed in damaged RPE. Although not well studied in human RPE, functional GLP-1R expression has been reported in cultured human RPE cells (ARPE-19).[25] Furthermore, GLP-1R has been detected in vascular endothelial cells,[26] suggesting expression in choroidal endothelium. Detecting GLP-1R by immunostaining is often challenging due to its wide distribution and antibody limitations.[59] Using thin paraffin sections of flat-mounted specimens, we successfully visualized the three-dimensional structure of small CNVs. This study is the first to document GLP-1R expression around mouse CNV using this approach.

Previous studies have reported GLP-1R expression in mouse eye tissue using PCR[26,60]; we also detected it in posterior tissue, although levels were low and varied among individuals. No significant expression changes were detected before or after laser stimulation or GLP-1R agonist

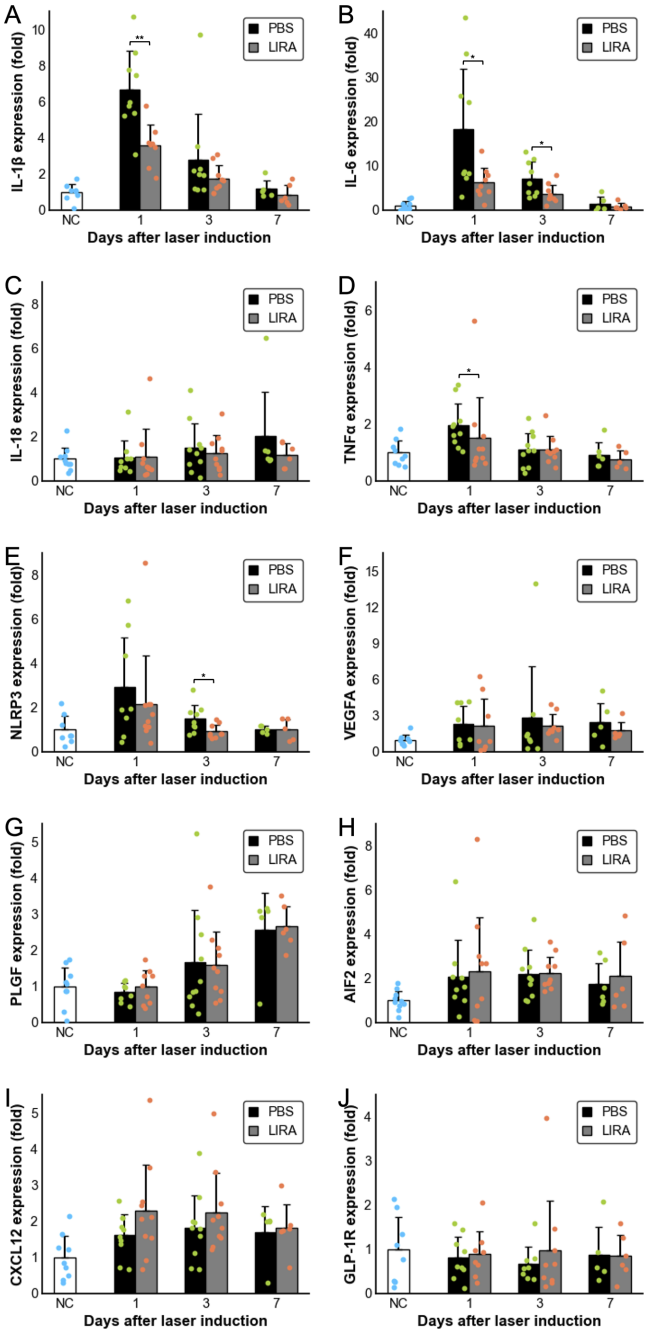

Figure 5. RT-qPCR analysis of inflammatory cytokines, migration-related proteins, GLP-1R, and NLRP3 expression in posterior ocular tissues of laser-induced CNV mice shows relative expression levels as bar graphs compared to untreated controls (day 0); *black bars* represent PBS-treated mice, and *gray bars* indicate mice treated daily with subcutaneous Liraglutide (1000 µg/kg) from post-laser day 0 to day 6; tissues were collected on days 1, 3 (n = 8–10), and 7 (n = 5–6); data are presented as mean ± SD, and differences between PBS and Liraglutide groups were assessed using the Mann–Whitney U test, with significance marked as $^{*}P < 0.05$ and $^{**}P < 0.01$. (**A**) IL-1β, (**B**) IL-6, (**C**) IL-18, (**D**) TNFα, (**E**) NLRP3, (**F**) VEGFA, (**G**) PLGF, (**H**) AIF2, (**I**) CXCL12, and (**J**) GLP-1R. AIF, apoptosis-inducing factor; CNV, choroidal neovascularization; CXCL12, C-X-C motif chemokine ligand 12; GLP-1R, glucagon-like peptide-1 receptor; IL, interleukin; NLRP3, NOD-like receptor protein 3; PBS, phosphate-buffered saline; PLGF, placental growth factor; RT-qPCR, reverse transcription polymerase chain reaction; SCI, subcutaneous injections; TNF, tumor necrosis factor; VEGFA, vascular endothelial growth factor A.

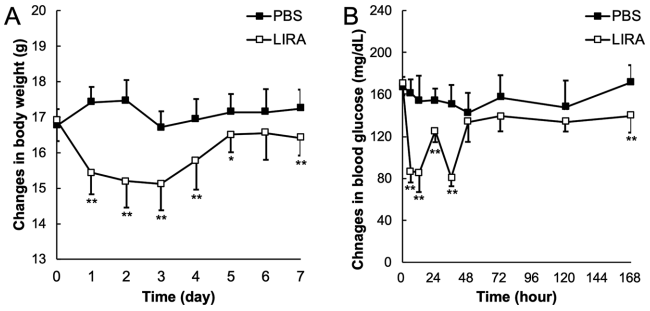

Figure 6. Changes in body weight (**A**) and blood glucose (**B**) over 7 days in mice administered PBS or subcutaneous Liraglutide (1000 µg/kg, n =10), with timepoint 0 marking the time of administration; body weight was recorded every 24 hours, whereas blood glucose was measured at 6, 12, 24, 36, and 48 hours, and then daily; *solid lines* represent the Liraglutide group (LIRA) means, *dotted lines* indicate PBS controls; data are shown as mean ± SD, and group differences were assessed by Mann–Whitney U test, with significance denoted as $^{*}P < 0.05$ and $^{**}P < 0.01$. PBS, phosphate-buffered saline.

treatment. This variability may reflect global inflammation from laser damage, rather than localized changes near the lesion.

NLRP3 Expression

NLRP3 contributes to AMD pathogenesis as part of the inflammatory pathway.[43,44] In a VEGF-A-induced AMD model, NLRP3 activation was suggested to suppress VEGF-A-induced AMD,[42] whereas knockout mouse studies showed reduced CNV formation.[61] NLRP3 promotes CNV by converting IL-1β to its active form and inducing inflammation while also producing IL-18, which suppresses CNV.[62] The stronger CNV-promoting effect of IL-1β likely outweighs IL-18's suppressive role, explaining the apparent contradiction.

In our study, NLRP3 was induced near CNV lesions after laser treatment, implicating the inflammasome pathway in this model. IL-1β expression increased alongside NLRP3, whereas IL-18 mRNA remained unchanged. The limited post-laser time points suggest that more frequent or extended monitoring may reveal further dynamics. Liraglutide down-regulated NLRP3, IL-1β, IL-6, and TNF, suggesting a role for the GLP-1–NLRP3 pathway in regulating intraocular inflammation and CNV formation.

Mechanism of Action of GLP-1

In our experiments, continuous subcutaneous Liraglutide injections suppressed inflammatory cytokine elevation in laser-treated tissue. GLP-1R, a membrane-bound G protein-coupled receptor, activates adenylate cyclase via Gαs coupling, increasing cAMP and initiating cell-specific responses.[63] However, the mechanism of GLP-1 action remains complex and debated. GLP-1 has shown anti-inflammatory effects via AMPK in HAECs[48] but conversely induces angiogenesis in HUVECs.[64,65] In our sprouting assay, angiogenesis was suppressed. This apparent contradiction may result from the assay's inclusion of various cell types—pericytes, microglia, and macrophages—not just endothelial cells.[45] Notably, when immune cells such as microglia and macrophages were depleted using clodronate liposomes, Liraglutide's anti-angiogenic effect disappeared.

These results suggest immune cells are essential to GLP-1's anti-angiogenic action.

The relationship between VEGF signaling and GLP-1 remains controversial. Some studies suggest GLP-1 suppresses VEGF in diabetic models[30] and mediates anti-angiogenic effects[26] through eNOS or MAPK/ERK[34] pathways,[36] whereas others found no direct interaction. In our study, Liraglutide had little to no impact on VEGF levels.

Direct and Indirect Effects of GLP-1R

Liraglutide stimulation involves both direct mechanisms—through GLP-1R-expressing immune and vascular endothelial cells—and indirect mechanisms—through glycemic control and weight loss.[58] In our study, blood glucose and body weight changes suggest indirect action. However, subcutaneous Liraglutide's CNV-suppressing effect was nullified by intravitreal GLP-1R antagonist, confirming intraocular GLP-1R involvement. The efficacy of intravitreal Liraglutide supports this direct mechanism. Additional evidence includes reports of topical GLP-1 treatments, such as eye drops.[22]

Liraglutide Dosing Concentrations and Safety

In vitro Liraglutide stimulation typically uses 100 nM, based on the manufacturer's monograph corresponding to a 1.8 mg/day human dose.[66] Moreover, dose-dependent effects have been reported between 50 and 2000 nM.[64] In our study, 100 nM had no significant effect in the sprouting assay, whereas 1000 nM induced strong anti-angiogenic and anti-inflammatory responses.

Rodent safety studies confirm tolerability up to 2000 µg/kg. The clinical human dose (15–30 µg/kg) translates to approximately 200 to 400 µg/kg in mice. Herein, 250 to 1000 µg/kg was used. At 1000 µg/kg, rapid weight loss occurred—a known GLP-1R agonist effect linked to its anti-obesity mechanism.[67,68] No severe hypoglycemia was observed, confirming short-term safety.[29]

Limitations

This study has methodological limitations in evaluating the GLP-1 signaling pathway. To confirm whether GLP-1R agonists directly affect NLRP3 or downstream cytokines, knockout models and gene silencing would be informative. ELISA and multiplex assays are also needed to assess protein expression.

The systemic effects of GLP-1 cannot be excluded. Metabolic conditions like diabetes and obesity, which promote angiogenesis, may have influenced results. Investigating these would require glycemic control approaches, such as calorie restriction or insulin, although such interventions may also alter CNV formation, complicating interpretation.

The laser-induced CNV model partially replicates AMD pathology. Unlike chronic degeneration in exudative AMD, laser injury causes acute Bruch's membrane disruption, creating an inflammatory environment that may have amplified GLP-1R agonist effects. Although low-dose intravitreal liraglutide was less effective than direct VEGFR inhibition, we do not propose it as a replacement for anti-VEGF drugs. However, GLP-1R agonists are safe, low-cost, and can be administered orally or subcutaneously. Their anti-inflammatory and anti-angiogenic properties may offer complementary benefits, potentially reducing treatment burden.

Despite these limitations, our findings show that GLP-1R agonists suppress CNV formation, likely via intraocular mechanisms involving immune cell modulation and NLRP3-cytokine pathway suppression. These results support GLP-1R agonists as promising complementary therapies for exudative AMD.

Acknowledgments

The authors thank Yumiko Tsunenari, a research assistant in the Department of Ophthalmology, Nagasaki University, for her thoughtful assistance with the preparation and coordination of experimental materials, as well as her skilled support in animal handling. The authors also wish to thank Kohei Harada and Diya Tang of the same department for their valuable technical advice regarding experimental techniques.

Supported by a grant-in-aid for scientific research (no. 22K09793) from the Japan Society for the Promotion of Science, Tokyo, Japan.

Disclosure: **A. Machida**, Chugai Pharmaceutical Co., Ltd. (Tokyo, Japan) (F); **K. Suzuki**, None; **T. Nakayama**, None; **S. Miyagi**, None; **Y. Maekawa**, None; **R. Murakami**, None; **M. Uematsu**, None; **T. Kitaoka**, Bayer Yakuhin, Ltd. (Osaka, Japan) (F), Novartis Pharma K.K. (Tokyo, Japan) (F), and Santen Pharmaceutical Co., Ltd. (Tokyo, Japan) (F), Santen Pharmaceutical Co., Ltd. (Tokyo, Japan) (F); **A. Oishi**, Bayer Yakuhin, Ltd. (Osaka, Japan) (F), Santen Pharmaceutical Co., Ltd. (Tokyo, Japan) (F), and Novartis Pharma K.K. (Tokyo, Japan) (F), Santen Pharmaceutical (F), Chugai (F), and Kowa (F)

References

1. Bressler NM. Age-related macular degeneration is the leading cause of blindness. *JAMA*. 2004;291:1900–1901.
2. de Jong PT. Age-related macular degeneration. *N Engl J Med*. 2006;355:1474–1485.
3. Lim LS, Mitchell P, Seddon JM, Holz FG, Wong TY. Age-related macular degeneration. *Lancet*. 2012;379:1728–1738.
4. Brown DM, Kaiser PK, Michels M, et al. Ranibizumab versus verteporfin for neovascular age-related macular degeneration. *N Engl J Med*. 2006;355:1432–1444.
5. Rosenfeld PJ, Brown DM, Heier JS, et al. Ranibizumab for neovascular age-related macular degeneration. *N Engl J Med*. 2006;355:1419–1431.
6. Investigators IS, Chakravarthy U, Harding SP, et al. Ranibizumab versus bevacizumab to treat neovascular age-related macular degeneration: one-year findings from the IVAN randomized trial. *Ophthalmology*. 2012;119:1399–1411.
7. Dugel PU, Koh A, Ogura Y, et al. HAWK and HARRIER: phase 3, multicenter, randomized, double-masked trials of brolucizumab for neovascular age-related macular degeneration. *Ophthalmology*. 2020;127:72–84.
8. Heier JS, Khanani AM, Quezada Ruiz C, et al. Efficacy, durability, and safety of intravitreal faricimab up to every 16 weeks for neovascular age-related macular degeneration (TENAYA and LUCERNE): two randomised, double-masked, phase 3, non-inferiority trials. *Lancet*. 2022;399:729–740.
9. Falavarjani KG, Nguyen QD. Adverse events and complications associated with intravitreal injection of anti-VEGF agents: a review of literature. *Eye (Lond)*. 2013;27:787–794.
10. Xu K, Chin EK, Bennett SR, et al. Endophthalmitis after intravitreal injection of vascular endothelial growth factor

inhibitors: management and visual outcomes. *Ophthalmology*. 2018;125:1279–1286.
11. Brown GC, Brown MM, Rapuano S, Boyer D. Cost-utility analysis of VEGF inhibitors for treating neovascular age-related macular degeneration. *Am J Ophthalmol*. 2020;218:225–241.
12. Lund PK, Goodman RH, Habener JF. Pancreatic preproglucagons are encoded by two separate mRNAs. *J Biol Chem*. 1981;256:6515–6518.
13. Schmidt WE, Siegel EG, Creutzfeldt W. Glucagon-like peptide-1 but not glucagon-like peptide-2 stimulates insulin release from isolated rat pancreatic islets. *Diabetologia*. 1985;28:704–707.
14. Kreymann B, Williams G, Ghatei MA, Bloom SR. Glucagon-like peptide-1 7-36: a physiological incretin in man. *Lancet*. 1987;2:1300–1304.
15. Drucker DJ, Nauck MA. The incretin system: glucagon-like peptide-1 receptor agonists and dipeptidyl peptidase-4 inhibitors in type 2 diabetes. *Lancet*. 2006;368:1696–1705.
16. Drucker DJ. Mechanisms of action and therapeutic application of glucagon-like Peptide-1. *Cell Metab*. 2018;27:740–756.
17. Pyke C, Heller RS, Kirk RK, et al. GLP-1 receptor localization in monkey and human tissue: novel distribution revealed with extensively validated monoclonal antibody. *Endocrinology*. 2014;155:1280–1290.
18. Deacon CF, Nauck MA, Toft-Nielsen M, Pridal L, Willms B, Holst JJ. Both subcutaneously and intravenously administered glucagon-like peptide I are rapidly degraded from the NH2-terminus in type II diabetic patients and in healthy subjects. *Diabetes*. 1995;44:1126–1131.
19. Batista AF, Forny-Germano L, Clarke JR, et al. The diabetes drug liraglutide reverses cognitive impairment in mice and attenuates insulin receptor and synaptic pathology in a non-human primate model of Alzheimer's disease. *J Pathol*. 2018;245:85–100.
20. Lu R, Yang J, Wei R, et al. Synergistic anti-tumor effects of liraglutide with metformin on pancreatic cancer cells. *PLoS One*. 2018;13:e0198938.
21. Tanday N, Flatt PR, Irwin N. Metabolic responses and benefits of glucagon-like peptide-1 (GLP-1) receptor ligands. *Br J Pharmacol*. 2022;179:526–541.
22. Hernandez C, Bogdanov P, Corraliza L, et al. Topical administration of GLP-1 receptor agonists prevents retinal neurodegeneration in experimental diabetes. *Diabetes*. 2016;65:172–187.
23. Cai X, Li J, Wang M, et al. GLP-1 treatment improves diabetic retinopathy by alleviating autophagy through GLP-1R-ERK1/2-HDAC6 signaling pathway. *Int J Med Sci*. 2017;14:1203–1212.
24. Hebsgaard JB, Pyke C, Yildirim E, Knudsen LB, Heegaard S, Kvist PH. Glucagon-like peptide-1 receptor expression in the human eye. *Diabetes Obes Metab*. 2018;20:2304–2308.
25. Puddu A, Sanguineti R, Montecucco F, Viviani GL. Retinal pigment epithelial cells express a functional receptor for glucagon-like peptide-1 (GLP-1). *Mediators Inflamm*. 2013;2013:975032.
26. Egholm C, Khammy MM, Dalsgaard T, et al. GLP-1 inhibits VEGFA-mediated signaling in isolated human endothelial cells and VEGFA-induced dilation of rat mesenteric arteries. *Am J Physiol Heart Circ Physiol*. 2016;311:H1214–H1224.
27. Zhang Y, Zhang J, Wang Q, et al. Intravitreal injection of exendin-4 analogue protects retinal cells in early diabetic rats. *Invest Ophthalmol Vis Sci*. 2011;52:278–285.
28. Fan Y, Liu K, Wang Q, Ruan Y, Zhang Y, Ye W. Exendin-4 protects retinal cells from early diabetes in Goto-Kakizaki rats by increasing the Bcl-2/Bax and Bcl-xL/Bax ratios and reducing reactive gliosis. *Mol Vis*. 2014;20:1557–1568.
29. Zeng Y, Yang K, Wang F, et al. The glucagon like peptide 1 analogue, exendin-4, attenuates oxidative stress-induced retinal cell death in early diabetic rats through promoting Sirt1 and Sirt3 expression. *Exp Eye Res*. 2016;151:203–211.
30. Sampedro J, Bogdanov P, Ramos H, et al. New insights into the mechanisms of action of topical administration of GLP-1 in an experimental model of diabetic retinopathy. *J Clin Med*. 2019;8:339.
31. Shu X, Zhang Y, Li M, et al. Topical ocular administration of the GLP-1 receptor agonist liraglutide arrests hyperphosphorylated tau-triggered diabetic retinal neurodegeneration via activation of GLP-1R/Akt/GSK3β signaling. *Neuropharmacology*. 2019;153:1–12.
32. Chung YW, Lee JH, Lee JY, et al. The anti-inflammatory effects of glucagon-like peptide receptor agonist lixisenatide on the retinal nuclear and nerve fiber layers in an animal model of early type 2 diabetes. *Am J Pathol*. 2020;190:1080–1094.
33. Dietrich N, Kolibabka M, Busch S, et al. The DPP4 inhibitor linagliptin protects from experimental diabetic retinopathy. *PLoS One*. 2016;11:e0167853.
34. Kolibabka M, Dietrich N, Klein T, Hammes HP. Anti-angiogenic effects of the DPP-4 inhibitor linagliptin via inhibition of VEGFR signalling in the mouse model of oxygen-induced retinopathy. *Diabetologia*. 2018;61:2412–2421.
35. Goncalves A, Lin CM, Muthusamy A, et al. Protective effect of a GLP-1 analog on ischemia-reperfusion induced blood-retinal barrier breakdown and inflammation. *Invest Ophthalmol Vis Sci*. 2016;57:2584–2592.
36. Zhou L, Xu Z, Oh Y, et al. Myeloid cell modulation by a GLP-1 receptor agonist regulates retinal angiogenesis in ischemic retinopathy. *JCI Insight*. 2021;6:e93382.
37. Lee YS, Jun HS. Anti-inflammatory effects of GLP-1-based therapies beyond glucose control. *Mediators Inflamm*. 2016;2016:3094642.
38. Reed J, Bain S, Kanamarlapudi V. Recent advances in understanding the role of glucagon-like peptide 1. *F1000Res*. 2020;9:F1000 Faculty Rev-239.
39. Puddu A, Maggi D. Anti-inflammatory effects of GLP-1R activation in the retina. *Int J Mol Sci*. 2022;23:12428.
40. Chen X, Huang Q, Feng J, Xiao Z, Zhang X, Zhao L. GLP-1 alleviates NLRP3 inflammasome-dependent inflammation in perivascular adipose tissue by inhibiting the NF-kappaB signalling pathway. *J Int Med Res*. 2021;49:300060521992981.
41. Hur J, Kang JY, Kim YK, Lee SY, Lee HY. Glucagon-like peptide 1 receptor (GLP-1R) agonist relieved asthmatic airway inflammation via suppression of NLRP3 inflammasome activation in obese asthma mice model. *Pulm Pharmacol Ther*. 2021;67:102003.
42. Marneros AG. NLRP3 inflammasome blockade inhibits VEGF-A-induced age-related macular degeneration. *Cell Rep*. 2013;4:945–958.
43. Tseng WA, Thein T, Kinnunen K, et al. NLRP3 inflammasome activation in retinal pigment epithelial cells by lysosomal destabilization: implications for age-related macular degeneration. *Invest Ophthalmol Vis Sci*. 2013;54:110–120.
44. Marneros AG. Role of inflammasome activation in neovascular age-related macular degeneration. *FEBS J*. 2021;290:28–36.
45. Shao Z, Friedlander M, Hurst CG, et al. Choroid sprouting assay: an ex vivo model of microvascular angiogenesis. *PLoS One*. 2013;8:e69552.
46. Tomita Y, Shao Z, Cakir B, Kotoda Y, Fu Z, Smith LEH. An ex vivo choroid sprouting assay of ocular microvascular angiogenesis. *J Vis Exp*. 2020;162:61677.
47. Jing Yin J, Bo Li Y, Ming Cao M, Wang Y. Liraglutide improves the survival of INS-1 cells by promot-

ing macroautophagy. *Int J Endocrinol Metab*. 2013;11:184–190.
48. Krasner NM, Ido Y, Ruderman NB, Cacicedo JM. Glucagon-like peptide-1 (GLP-1) analog liraglutide inhibits endothelial cell inflammation through a calcium and AMPK dependent mechanism. *PLoS One*. 2014;9:e97554.
49. Van Rooijen N. The liposome-mediated macrophage 'suicide' technique. *J Immunol Methods*. 1989;124:1–6.
50. van Rooijen N. Liposome-mediated elimination of macrophages. *Res Immunol*. 1992;143:215–219.
51. Schneider CA, Rasband WS, Eliceiri KW. NIH Image to ImageJ: 25 years of image analysis. *Nat Methods*. 2012;9:671–675.
52. Ryan SJ. The development of an experimental model of subretinal neovascularization in disciform macular degeneration. *Trans Am Ophthalmol Soc*. 1979;77:707–745.
53. Shah RS, Soetikno BT, Lajko M, Fawzi AA. A mouse model for laser-induced choroidal neovascularization. *J Vis Exp*. 2015;106:e53502.
54. Gong Y, Li J, Sun Y, et al. Optimization of an image-guided laser-induced choroidal neovascularization model in mice. *PLoS One*. 2015;10:e0132643.
55. Green BD, Irwin N, Gault VA, Bailey CJ, O'Harte FP, Flatt PR. Chronic treatment with exendin(9-39)amide indicates a minor role for endogenous glucagon-like peptide-1 in metabolic abnormalities of obesity-related diabetes in ob/ob mice. *J Endocrinol*. 2005;185:307–317.
56. Livak KJ, Schmittgen TD. Analysis of relative gene expression data using real-time quantitative PCR and the 2(-Delta Delta C(T)) method. *Methods*. 2001;25:402–408.
57. Kanda Y. Investigation of the freely available easy-to-use software 'EZR' for medical statistics. *Bone Marrow Transplant*. 2013;48:452–458.
58. Bendotti G, Montefusco L, Lunati ME, et al. The anti-inflammatory and immunological properties of GLP-1 receptor agonists. *Pharmacol Res*. 2022;182:106320.
59. Biggs EK, Liang L, Naylor J, et al. Development and characterisation of a novel glucagon like peptide-1 receptor antibody. *Diabetologia*. 2018;61:711–721.
60. Zhai R, Xu H, Hu F, Wu J, Kong X, Sun X. Exendin-4, a GLP-1 receptor agonist regulates retinal capillary tone and restores microvascular patency after ischaemia-reperfusion injury. *Br J Pharmacol*. 2020;177:3389–3402.
61. McGeough MD, Wree A, Inzaugarat ME, et al. TNF regulates transcription of NLRP3 inflammasome components and inflammatory molecules in cryopyrinopathies. *J Clin Invest*. 2017;127:4488–4497.
62. Doyle SL, Campbell M, Ozaki E, et al. NLRP3 has a protective role in age-related macular degeneration through the induction of IL-18 by drusen components. *Nat Med*. 2012;18:791–798.
63. Graaf C, Donnelly D, Wootten D, et al. Glucagon-like peptide-1 and its class B G protein-coupled receptors: a long march to therapeutic successes. *Pharmacol Rev*. 2016;68:954–1013.
64. Aronis KN, Chamberland JP, Mantzoros CS. GLP-1 promotes angiogenesis in human endothelial cells in a dose-dependent manner, through the Akt, Src and PKC pathways. *Metabolism*. 2013;62:1279–1286.
65. Kang HM, Kang Y, Chun HJ, Jeong JW, Park C. Evaluation of the in vitro and in vivo angiogenic effects of exendin-4. *Biochem Biophys Res Commun*. 2013;434:150–154.
66. Novo Nordisk Canada Inc. *Product monograph: including patient medication information*. Victoza/Liraglutide. Mississauga, Ontario; Novo Nordisk Canada Inc. Available at: https://www.novonordisk.ca/content/dam/Canada/AFFILIATE/www-novonordisk-ca/OurProducts/PDF/victoza-product-monograph.pdf. 2020.
67. Davies M, Færch L, Jeppesen OK, et al. Semaglutide 2·4 mg once a week in adults with overweight or obesity, and type 2 diabetes (STEP 2): a randomised, double-blind, double-dummy, placebo-controlled, phase 3 trial. *Lancet*. 2021;397:971–984.
68. Drucker DJ. GLP-1 physiology informs the pharmacotherapy of obesity. *Mol Metab*. 2022;57:101351.

Investigative Ophthalmology & Visual Science